EUROPEAN ORGANIZATION FOR NUCLEAR RESEARCH

CERN-EP/89-130
October 6th, 1989

REAL-TO-IMAGINARY RATIO FOR THE $\bar{p}$-NUCLEON FORWARD AMPLITUDE FROM LOW ENERGY $\bar{p}$-NUCLEUS DATA AND APPLICABILITY OF THE GLAUBER THEORY

G. Bendiscioli[1], A. Rotondi[1] and A. Zenoni[2,a]

1) Dipartimento di Fisica Nucleare e Teorica, Università di Pavia and Sezione I.N.F.N. di Pavia, Italy
2) CERN/EP, Geneva, Switzerland

ABSTRACT

Recent analyses of the antiproton-nucleus scattering below 600 MeV/c within the frame of the Glauber model are reviewed and discussed in their ability in determining unambiguously the antiproton–nucleon scattering parameters, in particular the ratio ρ_n = Re $f_n(0)$/Im $f_n(0)$ for the antiproton–neutron scattering amplitude. Also in the light of new data, the model is confirmed to work well at 600 MeV/c, while it loses reliability at 300 MeV/c. At this momentum it reproduces well total cross sections and the gross features of differential cross sections, but not their behaviour in the minima. Consequently it allows to determine the scattering amplitude parameters σ_n and β^2_n, but not ρ_n.

(Submitted to Nuclear Physics)

---

a) On leave of absence from 1)

1. INTRODUCTION

In recent years new evaluations of the real-to-imaginary ratio (ρ_p) of the antiproton-proton ($\bar{p}p$) forward elastic scattering amplitude have been carried out at the LEAR facility of CERN from small angle Coulomb interference measurements at $\bar{p}$ momenta between 180 and 1077 MeV/c [1,4] and measurements of shifts and widths of antiprotonic atom levels at rest [5-9]. These results join to pre-LEAR measurements [10-14] above 350 MeV/c.

According to [13], the interest in the determination of the ρ_p parameter at low momenta comes from various reasons. A straightforward search for the characteristic resonant structure is related to the issue of baryonium states near threshold. On the other hand, the global behaviour of ρ_p is related to the high-energy behavior of pp and $\bar{p}p$ total cross sections as well as to the imaginary part of the $\bar{p}p$ amplitude in the unphysical region, via the forward dispersion relation. In particular, the behavior of ρ_p at low momenta is sensitively dependent on the contribution from the high-mass region of the unphysical cut, and therefore provides a means to investigate the analytic structure of the $\bar{N}N$ scattering amplitude in the unphysical region where a direct measurement of the amplitude is impossible, and where no strictly quantitative theory of the scattering amplitude exists. The real-to-imaginary ratio at low momenta can be also compared with the predictions of potential models for the low-energy $\bar{N}N$ system, and therefore offers a means of testing or constraining these models.

In fig. 1 the values of the ρ_p parameter determined from small angle Coulomb interference measurements of $\bar{p}p$ scattering at incident momenta below 0.8 GeV/c are shown together with the value determined at rest by measurements of shifts and widths of antiprotonic atom levels. The figure shows a considerable spread of the values; this can in part be explained by the fact that a unique procedure for extracting ρ_p from the measured data does not exist, and there are many different assumptions - mainly in the parametrization of the $\bar{p}p$ differential cross-section - that determine large variations in ρ_p, whilst a meaningful comparison certainly requires a unified treatment [3]. Nevertheless the data seem to display an overall trend given by negative values at rest, positive values around 200 MeV/c, a decrease towards negative values between 200 and 400 MeV/c and positive values at higher momenta. Particularly noteworthy is the variation in ρ_p for momenta in the region between 150 and 400 MeV/c which is not predicted by potential models [8].

A contribution to the clarification of this open question came recently within the frame of the Glauber theory. In a number of papers [15-18] the applicability of this theory (normally utilized for the analysis of high energy hadron-nucleus scattering) to the low energy $\bar{p}$-nucleus scattering has been shown and the theoretical motivations extensively studied [19-23]. The theory includes both ρ_p and the correspondent ratio ρ_n for the antiproton-neutron ($\bar{p}n$) interaction. In ref. [15] the analysis of scattering data at 600 and 300 MeV/c on ^{12}C, ^{40}Ca, ^{208}Pb [24-29] led to the determination of the values of the $\rho=\rho_p=\rho_n$ parameter for the $\bar{p}$-nucleon forward scattering amplitude at the two momenta. The method

proposed for finding the values of ρ is based on the high sensitivity to ρ of the values of the differential cross sections at the diffractive minima; indeed, as shown in [15], in the absence of Coulomb scattering the cross section magnitude at diffractive minima is proportional to ρ^2. In the presence of Coulomb-nuclear interference the cross section at the diffractive minima depends on ρ in a more complicated way, but this dependence remains very strong; moreover, the cross section becomes sensitive to the sign of ρ. As a result of this analysis, at 300 MeV/c, the value ρ=0 for the $\bar{p}$-nucleon real-to-imaginary ratio is extracted from $\bar{p}$-nucleus elastic scattering data.

Recently [30] we have explored the possibility to analyse $\bar{p}$-nucleus elastic scattering data at low energy by means of a Glauber model with a different approach. Indeed we performed a fit on the $\bar{p}$-nucleus scattering data in order to extract, at the same time:

a) the $\bar{p}$-neutron scattering amplitude parameters having fixed from experimental data the $\bar{p}$-proton ones;
b) the degree of accuracy of the theory at low energy.

From our analysis of $\bar{p}$-nucleus data from [24-29] the following conclusions were drawn. At 600 MeV/c the validity of the Glauber theory for describing the $\bar{p}$-nucleus scattering has been shown and the parameters of the $\bar{p}$-neutron scattering amplitude have been determined. At 300 MeV/c, on the contrary, the presence of inaccuracies in the model have been detected; these inaccuracies make the theoretical predictions unreliable around the diffraction minima of the differential elastic cross section and consequently prevent to find unambiguously the value of the ρ_n through the fitting procedure. Hence, we concluded that at 300 MeV/c and below Glauber models must be considered as a tool for parametrizing in an effective way the diffractive behaviour of the $\bar{p}$-nucleus scattering distributions, but care is required in the attribution of a physical significance to the real-to-imaginary ratio of $\bar{p}$-nucleon amplitude derived from the data.

This last conclusion contradicts evidently the conclusions of ref. [15]. We felt that possible sources of this disagreement could be different mathematical procedures and different treatments of the data in the two analyses.

Indeed in ref. [15] some approximate formulas were used. In order to investigate the validity of these approximations, we calculated differential cross sections with our model (which does not make use of them) with the values of the input parameters as in ref. [15] and compared our results with the ones of ref. [15]. Also we put in evidence the incidence of some specific computational procedures or data treatments on the behaviour of the differential cross sections predicted by the model. This latter investigation showed that the use of approximate expressions, often given in the literature, for the phase of the Coulomb amplitude or the neglect of the smoothing of the theoretical curves over the finite resolution of the detector, affect strongly the values of the predicted cross sections at the minima.

In the mean time, we had a further confirmation that the Glauber theory becomes somewhat inaccurate at 300 MeV/c and below. Indeed, we verified that at this momentum the

impossibility to determine univocally the value of ρ_n does not depend on the uncertainty on the $\bar{p}$-proton parameters.

On the other side, the Glauber theory revealed to be effective in predicting total cross sections. So we examined its applicability at low energies by comparing its predictions to $\bar{p}$-nucleus reaction cross section data down to 200 MeV/c.

This paper is organized as follows. In Sect. 2 the Glauber theory is summarized and the main differences between the approaches of ref. [15] and of ref. [30] are put in evidence. In sect. 3 differential elastic cross sections are calculated by means of the model of ref. [30] but with the values of the parameters adopted in ref. [15]; the results are compared with those of ref. [15] and with experimental data. Possible reasons of the disagreement between the present results and those of ref. [15] are examined. In sect. 4 the full validity of the Glauber theory at 600 MeV/c and its limited validity at 300 MeV/c stressed in ref. [30] are reexamined in the light of new data. In Sect. 5 reaction cross sections are calculated by using the $\bar{p}$-nucleon parameters carried out from $\bar{p}$-nucleus elastic scattering and compared to experimental data. In Sect. 6 the reaction cross sections of $\bar{p}$ on ^{3}He and ^{4}He at 200 MeV/c are discussed. Sect. 7 contains our main conclusions.

2. THE GLAUBER MODELS

The model utilized in the work of ref. [30] is the same Glauber model [31] which describes successfully the p-nucleus scattering data at 1 GeV. Practically it consists of the eikonal approximation to the first order, assuming for the nucleus the independent particle model without antisimmetrization of the wave function and taking into account the Coulomb interaction in the average Coulomb field approximation.

The $\bar{p}$-nucleus scattering amplitude is given by: [30]

$$F_N(q) = iK \int J_0 (qb) [1 - D(b)] \, bdb \qquad (2.1)$$

with

$$D(b) = \prod_1^A {}_j \left[1 - \frac{1}{iK} \int J_o(tb) S_j(t) f_j(t) \, tdt \right] \qquad (2.2)$$

In these equations b is the impact parameter, K and q are the laboratory incident and transferred momenta, respectively, J_0 is the Bessel function, S_j is the nuclear form factor of the j-th nucleon and $f_j(q)$ the scattering amplitude of the $\bar{p}$ on that nucleon.

The form factor is expressed by:

$$S_j(q) = \int \exp(i\mathbf{q}.\mathbf{r}_j) \, \rho \, (\mathbf{r}_j) d^3 r_j \qquad (2.3)$$

where $\rho(r_j)$ is the density of the j-th nucleon.

The $\bar{p}$-nucleon scattering amplitude is parametrized in the usual form [31,32]:

$$f_j(q) = \frac{K}{4\pi}\sigma_j(\rho_j + i)\, e^{-\frac{1}{2}\beta_j^2 q^2} \qquad (2.4)$$

where j stands for neutron or proton (j=n,p), σ_j is the $\bar{p}$-nucleon total cross section, β^2_j is the slope parameter and ρ_j=Ref$_j$(0)/Imf$_j$(0).

The most relevant effects not accounted for in the model are: non eikonal effects, Pauli and spin correlations, effects due to the approximate treatment of the Coulomb interaction and of the center of mass constraint for heavy nuclei. These effects are expected to be small at low transferred momenta (small angles). In order to avoid in the calculations spurious effects due to inaccurate computation tecniques or approximations of exact formulae, all the calculations have been performed using analytical formulae whenever possible and solving numerically the basic formulae of the model in the other cases.

In ref. [15] the so called large-A approximation of the same Glauber model was utilized. The expression of the nuclear amplitude is as follows:

$$F_N(q) = iK\int_0^\infty \Gamma(b) J_o(qb) b\, db \qquad (2.5)$$

where $J_o(qb)$ is the Bessel function,

$$\Gamma(b) = 1 - \exp(i\chi_j(b)), \qquad (2.6)$$

$$\chi_j(b) = \frac{A}{2\pi K}\int e^{-iq.b} f_j(q)\, \phi(q) d^2q, \qquad (2.7)$$

$\phi(q)$ is the elastic nuclear form factor and f_j is the nucleon scattering amplitude (2.4). This approximation is derived [33] under the hypothesis that the range of the elementary interaction is much smaller than the nuclear radius. In [31] the authors suggest the use of the approximate formula only for heavier nuclei (Al, Cu, Pb), so the approximation seems to be inappropriate for the analysis of $\bar{p}$-^{12}C scattering data.

2.1 The input parameters

In ref. [30] the $\bar{p}$-proton scattering amplitude parameters and the nuclear shapes were the input parameters of the calculation. The former were taken from empirical formulae which

interpolate experimental data, the latter from nuclear charge distribution data. Harmonic oscillator single particle densities were adopted for light nuclei (A<16), Wood-Saxon densities for heavy nuclei. The $\bar{p}$-neutron scattering amplitude parameters were left as free parameters of the fitting procedure.

In ref. [15] the nuclear parameters for ^{12}C and ^{40}Ca are close to those in ref. [30]. The same holds for the $\bar{p}$-proton scattering amplitude parameters with the exception of the ρ_p parameter at 300 MeV/c. At this energy the two values ρ_p=0.0 and ρ_p=-0.25 were utilized and the former was found to be in better agreement with the experimental data. Concerning the $\bar{p}$-neutron scattering amplitude parameters, the total $\bar{p}$-neutron cross section (σ_n) was deduced from $\bar{p}$-deuteron total cross section taking into account the Glauber correction for screening, whereas for the slope parameter (β^2_n) and the real-to-imaginary ratio (ρ_n) assumptions were made for their values. Indeed both β^2_n and ρ_n were considered equal to the corresponding parameters for the $\bar{p}$-proton scattering amplitude. Therefore in ref. [15] the value of $\rho=\rho_p=\rho_n$ and $\beta^2=\beta^2_n=\beta^2_p$ parameters have to be considered as an average between the proton and neutron parameters.

In tables I and II a summary of the two sets of input parameters is shown.

2.2 Data analysis.

In ref. [30] the $\bar{p}$-neutron scattering amplitude parameters were extracted by means of a fitting procedure from the $\bar{p}$-^{12}C, $\bar{p}$-^{40}Ca elastic scattering data at 300 MeV/c and from the $\bar{p}$-^{12}C, $\bar{p}$-^{16}O, $\bar{p}$-^{40}Ca elastic scattering data at 600 MeV/c. The degree of accuracy of the theory at the different energies was investigated by means of the statistical compatibility among the best fit values of the $\bar{p}$-neutron amplitude parameters for different nuclei at the same energy. At 300 MeV/c the ρ_n values extracted from ^{12}C and ^{40}Ca data are statistically incompatible, so the value carried out by fitting simultaneously the data from both nuclei is doubtful. The $\bar{p}n$ parameters are shown in tab. II.

In fig. 2 the comparison between experimental data on $\bar{n}$-proton (which is the same as $\bar{p}$-neutron) total cross section [36] and the values extracted from the analysis at 300 and 600 MeV/c is shown. For the other two $\bar{p}$-neutron parameters no experimental data are available.

In ref. [15] no fit was performed. The agreement between theory and experimental data was estimated by comparing by sight the theoretical curves and the experimental points. At 300 MeV/c this procedure led to choose between two possible values of the $\rho=\rho_p=\rho_n$ parameter: ρ=-0.25 (pre-LEAR data [12]) and ρ=0.0 (LEAR data [1,2]).With the value ρ=0.0 the theory reproduces with better accuracy the experimental data. In figs. 3 and 4 the figures from the original work are shown.

The differences between the two approaches of ref. [30] and ref. [15] make difficult a direct comparison of the results. Anyway, it is evident that different conclusions have been drawn from the two analyses concerning the applicability of the Glauber theory at the lowest momentum 300 MeV/c. A clarification of the possible reasons of this disagreement could be

useful also to enlighten the interesting question of the low energy limit of applicability of the Glauber theory to $\bar{p}$-nucleus data.

3. POSSIBLE REASONS OF DISAGREEMENT BETWEEN THE TWO MODELS

To this aim the attempt was made to calculate the same differential cross sections as in ref. [15] by means of the model of ref. [30] with the same input parameters of ref. [15] (see tab. I and II).

At 600 MeV/c the two models give different but not incompatible results. In Fig. 5 the results of the present analysis are shown for ^{12}C and ^{40}Ca; the two theoretical curves have to be compared with the corresponding curves of fig. 4 taken from ref. [15]. It is evident that fig. 4a and fig. 5a (^{12}C) are different expecially in the minima. The theoretical predictions for ^{40}Ca are more similar, apart from the minima. The better agreement for ^{40}Ca is probably due to the better effectiveness of the large-A approximation for ^{40}Ca than for ^{12}C. However, in spite of the differences, the predictions of the two models appear to agree with the data equally, if compared by sight, so that the same conclusions as those of ref. [15] can be drawn concerning the values of the nucleon input parameters.

At 300 MeV/c, on the contrary, the two models give different and incompatible results. In fig. 6 the results of the present analysis are shown for ^{12}C and ^{40}Ca; the theoretical curves have to be compared with the curves of fig. 3.

Also in this case the theoretical curves are more similar in the case of ^{40}Ca (figs. 3b and 6b) than in the case of ^{12}C (Figs. 3a and 6a), but in the minima of the distributions the theoretical predictions of the two models differ strongly for both nuclei. Comparing theoretical curves and experimental data by sight the present calculation, in agreement with ref. [30], leads to the conclusions that the best value for the ρ parameter depends on the sort of nucleus: ρ=0.0 for ^{12}C and ρ=-0.25 for ^{40}Ca, while in ref. [15] (see fig. 3) one concludes that the best value is 0 for both nuclei.

We examine in the following a certain number of possible reasons of disagreement between the predictions of the two models.

An established fact is that the large-A approximation used in ref. [15] gives different results from the full formulae used in ref. [30]. Considering, moreover, that the most relevant differencies between the predictions of the two models are found in the minima of the distributions, a number of aspects of the calculations can be remarked which affect mainly the behaviour of the cross section in the diffraction minima.

The first remark concerns the calculation of the Coulomb phase η for the Coulomb amplitude for the scattering of a particle of charge Z and velocity β by a point like nucleus (Formula (10) of ref. [30]):

$$\eta = \arg \Gamma (1+i\gamma) \qquad \gamma = Z/137\,\beta \qquad (3.1)$$

We verified that at 300 MeV/c the approximate expressions for η reported in refs. [31,32] give incorrect results also for light nuclei. The consequent inaccuracies affect mainly the values of the cross section in the diffraction minima. In ref. [30] the evaluation of η was performed numerically starting from the definition:

$$\Gamma(x) = \int_0^\infty t^{x-1}\, e^{-t}\, dt \qquad (3.2)$$

The second remark concerns the necessity of performing a smoothing of the theoretical curves before comparing them with experimental data. This procedure is necessary in order to account for the finite experimental acceptance of the apparatus. In ref. [37] the authors suggest the following formula for the averaging of theoretical cross sections:

$$\sigma_{th}(\theta) = \frac{1}{3}\left[\frac{d\sigma_{th}(\theta-\Delta\theta/\sqrt{2})}{d\Omega} + \frac{d\sigma_{th}(\theta)}{d\Omega} + \frac{d\sigma_{th}(\theta+\Delta\theta/\sqrt{2})}{d\Omega}\right] \qquad (3.3)$$

where $\Delta\theta$ is the experimental angular detection width. It is evident that the averaging of the theoretical cross sections has the effect of smoothing the depth of the minima.

The third remark concerns the necessity of considering in the calculations a different beam energy in the minimum of the ^{12}C distributions at 300 MeV/c. This is due to a different target thickness. We will not consider in detail this point in the following.

In order to show the effects of the two first points listed above on the predictions of the theory we have considered the case of ^{40}Ca, for which the predictions of the models of refs. [15] and [30] seem to agree better, owing to the better accuracy of the large-A approximation (see figs. 3b and 6b, figs. 4b and 5b).

Fig. 7 shows the theoretical curve for the $\bar{p}$-^{40}Ca elastic scattering at 600 MeV/c (in the same conditions as in fig. 5b) computed with and without the smoothing of the cross sections by formula (3.3). The effect of the approximation of the Coulomb phase is negligible at this energy and has not been considered. It is evident the effect of the smoothing in the minima of the distribution; the curves of fig. 7 have to be compared with the curve of fig. 4b from ref. [15].

The effect of the approximation of the Coulomb phase and of the smoothing of the theoretical values of the cross sections is more evident in the case of ^{40}Ca at 300 MeV/c. In fig. 8a) and b) the theoretical cross sections for ^{40}Ca at 300 MeV/c computed in the same condition as in fig. 6b (ρ=0.0 and ρ=-0.25 respectively) are compared with the theoretical cross sections obtained with the same calculations but without the smoothing of the data

(dotted lines) and also using the approximated formula for η reported in ref. [32] (dashed lines).

The effects at the minima of the treatment of the Coulomb phase and of the cross section averaging can be very important and could lead to completely different conclusions concerning the best value of the ρ parameter. Indeed, when our complete model is utilized, the best value of ρ is -0.25 (full line in fig. 8b). On the contrary, when the smoothing procedure is neglected and the approximate formula for the Coulomb phase is adopted, the best value of ρ is 0.0 (compare by sight or by χ^2 the dotted and dashed lines in figs. 8a and 8b; see also fig. 3b from ref. [15]).

The main conclusion is that, when information about the ρ parameter are extracted from a Glauber model calculation, care is necessary in reproducing cross section values in the minima of the distributions and in comparing them with the experimental data, since cross section values in diffractive minima are extremely sensitive to the values of the ρ parameter.

4. FURTHER TESTS OF THE GLAUBER THEORY

Following the results of ref. [30] the Glauber theory seems to work well at 600 MeV/c whereas it seems to be slightly inaccurate at 300 MeV/c.

In order to test further the results at 600 MeV/c, the differential elastic cross sections for ^{18}O and ^{208}Pb were reproduced using the best fit values for $\bar{p}$-neutron parameters. In the case of these nuclei uncertainties arise in the determination of the geometrical parameters of the nuclear matter distribution. For both nuclei Wood-Saxon charge and matter distributions are assumed but, owing to the different numbers of protons and neutrons, the assumption $R=R_{ch}$ [38] adopted for ^{12}C, ^{16}O and ^{40}Ca is no more allowed. For ^{18}O and ^{208}Pb electric charge distribution parameters are drawn from electromagnetic scattering experiments whereas for the matter distributions reasonable but arbitrary parameters are used (see tab. III). Nuclear parameters for ^{16}O (tab. I) and ^{18}O (tab. III) are not directly comparable since for the former nucleus harmonic oscillator single particle density has been adopted. Moreover for ^{208}Pb, due to the high electric charge of the nucleus, the approximate treatment of the Coulomb interaction (mean field approximation) should result in inaccuracies in the prediction of the theoretical cross section mainly at high transferred momenta. In fig. 9 theoretical predictions of the model are compared with experimental data. In spite of the uncertainties on the nuclear shape parameters for the two nuclei, the agreement is remarkably good.

At 300 MeV/c, where the model seems to exibit inaccuracies in the prediction of the depth of the minima, a further investigation on the consistency of the theory was made, based on a more constrained fit according to the following arguments:

a) at 300 MeV/c experimental data on the total $\bar{n}p$ ($\bar{p}n$) cross section do exist [36];

b) at the same energy, where the experimental value of ρ_p is uncertain (see Fig. 1), the

authors of ref. [15] suggest in ref. [40] that the value of ρ_p could be near 0.0 (instead of -0.132 utilized in the calculations of ref. [30]).

Hence a fit on ^{12}C and ^{40}Ca data at 300 MeV/c was performed fixing the value of the total $\bar{p}$-neutron cross section at the experimental value (214±13±12)mb, and the value of the real to imaginary ratio for the proton at zero and at -0.132. The other two parameters of the $\bar{p}$-neutron amplitude were left free. The results of the fit are shown in table IV. Also in this case it is evident that, no matter which value of ρ_p is adopted (0.0 or -0.132), the values of the ρ_n parameter extracted from separate fits on the ^{12}C and ^{40}Ca data are not statistically consistent.

In fig. 10 the result of the simultaneous fit on ^{12}C and ^{40}Ca is shown (row f of table IV). As in fig. 2 of [30] the inaccuracies of the theory are particularly evident in the minimum of the ^{12}C distribution. In conclusion, independently of the values of the proton input parameters, the theory seems to be not enough accurate to allow an unambiguous determination of the ρ_n parameter. This result suggests that at 300 MeV/c the Glauber theory could have a low energy limit of applicability for the $\bar{p}$-nucleus scattering data.

On the contrary, from table IV, it seems that the value of the slope parameter β^2_n has been very well determined by the fitting procedure. Indeed the values obtained for the β^2_n parameter for the two nuclei fit separately are very close. The value for β^2_n obtained from the contemporary fit of the two nuclei is 25.1±1.3 $(GeV/c)^{-2}$ (ρ_p=-0.132, row f of tab. IV).

It is important to remark that the values of the two parameters σ_n and β^2_n are inversely correlated; so increasing the value of σ_n, a correspondent decreasing of the value of β^2_n is obtained. Consequently, the best fit value obtained for β^2_n depends on the value assumed for the total cross section (the experimental value of which is affected by considerable statistic and sistematic errors). Indeed, varing the σ_n value within the statistical error (±13 mb), the central value of β^2_n varies from 27.5 $(GeV/c)^{-2}$ to 22.9 $(GeV/c)^{-2}$. In any case the consistency is not destroyed changing the value of σ_n.

The different behaviour of the two parameters ρ_n and β^2_n can be understood qualitatively considering that changes in the value of the ρ_n parameter affect mainly the depth of the minima of the distributions as it can be seen in fig. 6. The parameter β^2_n, on the contrary, together with the total cross section σ_n, defines the size of the neutron and consequently of the nucleus. Therefore it contributes to determine the gross features of the scattering distribution like the values of the cross section up to the first minimum and the position of the minima.

In conclusion, at 300 MeV/c, the Glauber theory seems to be effective in reproducing the main features of the scattering distributions (which depends on the β^2_n value) whereas it seems to be less accurate in predicting details of the distributions like the depth of the minima (which are particularly sensitive to the values of ρ_n).

5. ANALYSIS OF THE $\bar{p}$-NUCLEUS REACTION CROSS SECTIONS

The $\bar{p}$-nucleus reaction cross sections can be obtained in the framework of the Glauber theory by means of the optical theorem:

$$\sigma_R = \frac{4\pi}{K} \text{ Im } F_N(0) - 2\pi \int |F_N(\theta)|^2 \text{sen}\theta d\theta \qquad (5.1)$$

The integral contained in (5.1) is sensitive only to the behaviour of the scattering distributions up to the first diffraction minimum and not on details of the distribution like the depth of the minima, so that σ_R is not sensitive to the values of the ρ_n parameter (see also ref. [42]). Consequentely one can expect that the Glauber theory is able to reproduce correctly $\bar{p}$-nucleus reaction cross sections at low energy even if the theory results to be slightly inaccurate in reproducing all features of elastic scattering distributions.

In fig. 11 the reaction cross sections of antiprotons on several nuclei at three different momenta 600 MeV/c, 300 MeV/c, 200 MeV/c are shown. The reaction cross sections have been reproduced by means of formula (5.1). At 600 and 300 MeV/c the input parameters for the $\bar{p}$-proton amplitude and the best fit parameters for the $\bar{p}$-neutron amplitude of ref. [30] (see tab. II, part (a)) have been employed. The ρ_n parameter at 300 MeV/c has been also fixed at the best fit value -0.080, even if this value is not an unambiguous determination of ρ_n.

At 200 MeV/c the validity of the theory is somewhat questionable and the parameters of the elementary scattering amplitudes ($\bar{p}p$ and $\bar{p}n$) are not well known. A reasonable set of parameters for the $\bar{p}$-nucleon amplitudes has been adopted at this low energy; details concerning the choice of these parameters and considerations about the applicability of the theory are given in the next section.

At the three energies the nuclear shape parameters are reported in tab. V; for light nuclei (A<16) harmonic oscillator single particle densities were adopted, for heavy nuclei Wood-Saxon densities. The nuclear parameters were determined as described in ref. [30].

Fig. 11 shows that the agreement between experimental data and theoretical predictions is remarkably good at the three energies. Apparently the neon cross sections make exception, but it has to be remarked that the experimental values are lower limits, probably understimated by 5% [16]. Applying this correction to the data a very good overall agreement is obtained.

6. ^{3}He AND ^{4}He REACTION CROSS SECTIONS AT 200 MeV/c

In this section we analyse within the frame of the Glauber theory the reaction cross section $\bar{p}$-^{4}He at 192.8 MeV/c, $\sigma_R(^4\text{He})=405.6 \pm 16.4$ [43], and the reaction cross section $\bar{p}$-^{3}He at the same antiproton momentum, $\sigma_R(^3\text{He})=392.4 \pm 23.8$ [44]. The two cross sections are suprisingly close, in spite of the different numbers of nucleons present in the two nuclei. As stressed in the previous section, although at this very low momentum the validity of the theory is somewhat questionable, we expect it is able to give correct values for

integrated cross sections. Indeed some calculations reproduce data on deuterium satisfactorily [42].

Moreover, we recall that previous Glauber model calculations led to the following conclusions: (a) the experimental reaction cross section values on ^{4}He at 300 and 600 MeV/c are very well reproduced by the model; (b) the calculated reaction cross sections on ^{3}He at the above momenta are equal to the ^{4}He ones within 6% [44].

Hence, in the framework of the Glauber theory, at higher energies the equality $\sigma_R(^4He) \approx \sigma_R(^3He)$ is explainable in terms of a "geometrical effect" (that is, in ^{3}He the number of nucleons smaller than in ^{4}He is compensated by a smaller shadow effect due to the larger size of ^{3}He).

Of course, at very low energies, where few partial waves are involved in the $\bar{p}$-nucleon interaction, the parametrization of eq. (2.4), which is valid for a diffractive regime, should be substituted by a partial wave expansion. Also, the use of an amplitude obtained from some antiproton-nucleon potentials should be more appropriate.

Nevertheless, we calculated the $\bar{p}$-^{3}He reaction cross section at 200 MeV/c by eq. (5.1) having as input quantities the elementary scattering amplitudes defined by eq. (2.4). The six input parameters σ_j, ρ_j and β^2_j are determined as follows. The values of σ_p=334.0 mb and ρ_p=0.1 are taken from $\bar{p}p$ elastic scattering data [2], that of σ_n=274.0 mb from $\bar{n}p$ data [36]. The values of β^2_p measured around 200 MeV/c are affected by a large error. The interpolation of data from refs. [1] and [2] gives β^2_p=73±20 (GeV/c)$^{-2}$, whereas the extrapolation to lower energy, with an empirical formula, of higher energy data gives β^2_p=48(GeV/c)$^{-2}$ [41]. The values of β^2_n and ρ_n at 200 MeV/c are totally unknown. Since the total reaction cross section is nearly independent of ρ [42], we put $\rho_p=\rho_n$; moreover, since at 300 MeV/c the condition $\sigma_p/\sigma_n=\beta^2_p/\beta^2_n$ seems to hold [30] and is physically justified when ρ_p, ρ_n<<1 and the $\bar{p}$-nucleon amplitude is forward peaked [48], we put also

$$\beta^2_n = \beta^2_p(\sigma_n/\sigma_p) \qquad (6.1)$$

The radii of the distributions of the nucleon centers, which define in the Glauber model the size of the nucleus, have been fixed as R(^{4}He)=1.37 fm and R(^{3}He)=1.56 fm according to refs. [39] and [47], respectively.

In this way, all the input parameters are determined, except for β^2_p and β^2_n, so we made the calculations assuming for β^2_p both the values mentioned above (48 and 73 (GeV/c)$^{-2}$) and calculated β^2_n by eq. (6.1) and σ_R by eq. (5.1). The results are reported in tab. VI.

We see that a good agreement with the data is achieved for β^2_p=48 (GeV/c)$^{-2}$ and β^2_n=39 (GeV/c)$^{-2}$. Moreover, tab. VI shows that the calculated reaction cross sections on ^{3}He and ^{4}He are equal within 10% for both sets of input parameters utilized, in agreement with the measurements. This indicates that the equality $\sigma_R(^3He)=\sigma_R(^4He)$ is explainable by

assuming that in ^{3}He the number of nucleons lower than in ^{4}He is compensated by a smaller shadow effect due to the larger ^{3}He size. Of course, in the light of the above discussion on the reliability of the Glauber theory, the best values of β^2_n and β^2_p found here cannot be considered as a new determination of these two parameters.

7. CONCLUSIONS

The main conclusions of our analysis are the following.

When information on the ρ parameter is carried out from Glauber theory calculations, care is necessary in reproducing differential cross section values in the minima and in comparing them with experimental data, since they are very sensitive to the value of ρ. Two aspects of the calculations to be considered carefully are the approximations in the calculation of the Coulomb phase and the smoothing of the theoretical cross sections on the resolution of the detector.

As put in evidence also in a previous work, the Glauber theory becomes inaccurate in reproducing $\bar{p}$-nucleus elastic scattering distributions at low energy (say below 300 MeV/c). This is revealed by the impossibility of determining univocally (i.e., independently of the nucleus) the value of ρ_n. We have shown that this is not a consequence of uncertainties on ρ_p.

Nevertheless, the Glauber theory is able, also at low energy (300 MeV), to determine, within the limits of their correlation, the parameters β^2_n and σ_n.

This makes Glauber models effective in the calculation of $\bar{p}$-nucleus reaction cross sections, which depend more on the gross features of the differential cross sections (i.e., on β^2_n and σ_n) than on the details (i.e., on ρ_n). We verified that the model gives correct values of the reaction cross sections between 300 and 600 MeV/c for A=4-65 by using the parameters obtained by a best fit analysis of elastic scattering data. Good results have been obtained also at 200 MeV/c using a reasonable set of parameters for the $\bar{p}$-nucleon amplitude. Finally, we have analyzed ^{3}He and ^{4}He reaction cross sections at 200 MeV/c. Their equality seems to be explainable as a compensation between the different numbers of nucleons (3 against 4) in the two nuclei and their different sizes (larger for ^{3}He and smaller for ^{4}He).

REFERENCES

1. W. Brückner et al., Phys. Lett. 158B (1985) 180
2. L. Linssen et al., Nucl. Phys. A469 (1987) 726
3. P. Schiavon et al., CERN-EP/89-38
4. W. Brückner et al., Proc. 4th LEAR Workshop on Physics at LEAR with Low-Energy Antiprotons, eds. C. Amsler et al., Villars-sur-Ollon, 1987 (Harwood Academic Publ., London, 1988) p. 277.
5. S. Ahmad et al., Phys. Lett. B157 (1985) 333
6. T.P. Gorringe et al., Phys. Lett. B162 (1985) 71
7. M. Ziegler et al., Phys. Lett. B206 (1988) 151
8. C.W.E. Van Eijk et al., Nucl. Phys. A486 (1988) 604.
9. L.M. Simons, Proc. 4th LEAR Workshop on Physics at LEAR with Low-Energy Antiprotons, eds. C. Amsler et al., Villars-sur-Ollon, 1987 (Harwood Academic Publ., London, 1988) p. 703.
10. H. Kaseno et al., Phys. Lett. B61 (1976) 203
11. P. Jenni et al., Nucl. Phys. B94 (1975) 1
12. M. Cresti et al., Phys. Lett. B132 (1983) 209
13. H. Iwasaky et al., Phys. Lett. B103 (1981) 247, Nucl. Phys. A433 (1985) 580
14. V. Ashford et al., Phys. Rev. Lett. 54 (1985) 518
15. O.D. Dalkarov and V.A. Karmanov, Phys. Lett. 147BB (1984) 1; Nucl. Phys. A445 (1985) 579; Sov. Phys. JETP 62 (4) (1985) 645; Sov. J. Nucl. Phys. 45 (3) (1987) 430; Nucl. Phys. A478 (1988) 635c.
16. F. Balestra et al., Nucl. Phys. A452 (1986) 573
17. L.A. Kondratyuk and M.G. Sapozhnikov, Sov. J.Nucl. Phys. 46 (1987) 56
18. F. Balestra et al., Nucl. Phys. A 465 (1987) 714
19. D.R. Harrington, Phys. Rev. 184 (1969) 1745
20. V.M. Eisenberg, Ann. of Phys. 71 (1972) 542
21. S.J. Wallace, Adv. Nucl. Phys. 12 (1981) 135
22. V.B. Mandelzweig and S.J. Wallace, Phys. Rev. C25 (1982) 61
23. V.B. Belyaev and S.A. Rakityanskii, Sov. J. Nucl. Phys. 42 (1985) 867
24. D. Garreta et al., Phys. Lett. 135A (1984) 266
25. D. Garreta et al., Phys. Lett. 149B (1984) 64
26. D. Garreta et al., Phys. Lett. 151B (1985) 473
27. D. Garreta et al., Phys. Lett. 169B (1986) 14
28. M.C. Lemaire, Proc. of Int. Symp. on Nucleon and Antinucleon Scattering, Bad Honnef 1985, Lecture Notes in Physics 243 (1985) 285.
29. D. Garreta, Proc. of Third LEAR Workshop, Tignes 1985, eds. U. Gastaldi, R. Klapisch, J.M. Richard and J. Tran Thanh Van (Edition Frontières, 1985) p. 599

30. G. Bendiscioli et al., Nucl. Phys. A469 (1987) 669
31. R. Glauber and G. Matthiae, Nucl. Phys. B21 (1970) 135
32. G.D. Alkhazov, Nucl. Phys. A280 (1977) 330, G.D. Alkhazov et al., Phys. Rep. 42 (1978) 89
33. R.J. Glauber in: Lectures in theoretical physics ed. W.E. Brittin et al. (Interscience Publishers, New York, 1959) I, 315
34. A.S. Clough et al., Phys. Lett. B146 (1984) 299
35. D.V. Bugg et al., Phys. Lett. B194 (1987) 563
36. T. Armstrong et al., Phys. Rev. D36 (1987) 659
37. M.C. Lemaire et al., Nucl. Phys. A456 (1986) 557
38. G. Greenless, G.J. Pyle and Y.C. Tang, Phys. Rev. 171 (1968) 1115; G. Greenless, W. Makofske and G.J. Pyle, Phys. Rev. C1 (1970) 1145
39. R.C. Barrett and D.F. Jackson, Nuclear sizes and structures (Claredon, Oxford, 1977) pgs. 146-163.
40. O.D. Dalkarov, V.A. Karmanov, Proc. of the Fourth LEAR Workshop (Villars-Sur-Ollon, 1987), eds. C. Amsler et al. (Harwood Academic, New York, 1988), pg. 679
41. A. Zenoni, Proc. Fourth LEAR Workshop (Villars-sur-Ollon, 1987), eds. C. Amsler et al. (Harwood Academic, New York, 1988) pg. 669
42. L.A. Kondratyuk, M.G. Sapozhnikov, Sov. J. Nucl. Phys. 46 (1987) 56
43. F. Balestra et al., Phys. Lett. B165 (1985) 265
44. F. Balestra et al., Phys. Lett. B215 (1988) 247
45. F. Balestra et al., Nuovo Cimento A100 (1988) 323
46. K. Nakamura et al., Phys. Rev. Lett. 52 (1984) 731
47. A.V. Blinov et al., J. Phys. G, Nucl. Phys. 10 (1984) 727
48. L.A. Kondratyuk et al., Sov. J. Nucl. Phys. 33 (1981) 413

TABLE CAPTIONS

TAB. I

Nuclear shape parameters. For light nuclei ($A \leq 16$) harmonic oscillator single particle densities were adopted; for heavy nuclei ($A>16$) Wood-Saxon densities. R and a are the radius and the diffuseness parameter of the point-like nucleon distribution. R_{ch} and a_{ch} are similar quantities for the charge density.

TAB. II

Parameters of the $\bar{p}$-proton and $\bar{p}$-neutron elementary amplitudes at 300 and 600 MeV/c (See formula (2.4)). (†) Both values were used in the calculations; the former was chosen as the best. (*) Determined from the fit.

Data obtained al LEAR from $\bar{p}p$ scattering experiments have been published [34,35]. The proton parameters obtained from these measurements agree well with those given by us in this table, apart from a small difference in the σ_p values. Indeed, the best fit formula reported in [34,35] gives σ_p=245 mb at 300 MeV/c and σ_p=155 mb at 600 MeV/c (the statistical error is about 0.4%); these values are about 5-6 mb higher than those used here. If we use these new values in our fitting procedure, we obtain for σ_n values 5-6 mb lower than those reported here.

TAB. III

Nuclear shape parameters for ^{18}O and ^{208}Pb; Wood-Saxon densities have been adopted for of the two nuclei. For the meaning of the symbols see tab. I. The values of R_{ch} and a_{ch} are taken from [39].

For ^{18}O we fix $R=R_{ch}$ and choose a in order to have a r.m.s. radius of the point nuclear density of 2.74 fm. This value is the weighted average between the r.m.s. radii of the point charge density of ^{16}O (2.60 fm) and ^{20}Ne (2.88 fm). The r.m.s. radius of the point charge density is obtained from the relation $\langle r^2 \rangle - \langle r^2_p \rangle$ where $\langle r^2 \rangle$ is the charge m.s. radius and $\langle r^2_p \rangle = 0.69$ fm^2 is the m.s. radius of the proton charge density.

For Pb, the values of R_{ch} and a_{ch} correspond to a point charge density r.m.s. radius of 5.45 fm. The reported values of R and a give a nuclear r.m.s. radius of 5.84 fm. corresponding to a difference in the neutron and proton r.m.s. radii of 0.6 fm. This difference represents an upper limit for the so-called neutron excess in Pb (see for example, ref. [39] pag. 232).
Decreasing this difference down to zero, the χ^2 in fig. 9b increases by a factor up to two.

TAB. IV

Best fit values of β^2_n and ρ_n obtained at 300 MeV/c for two different values of ρ_p. The row indices in the energy column indicate that, in the fit on more nuclei each nucleus has

been considered at the proper energy of the incident $\bar{p}$. The error on the best fit values is the first standard deviation found by the minimization program taking fully into account the correlations between the parameters and the non-parabolic behaviour of the χ^2 function.

TAB. V

Nuclear shape parameters. For light nuclei ($A \leq 16$) harmonic oscillator single particle densitites were used; for heavy nuclei Wood-Saxon densitites. For the meaning of the symbols see tab. I. The numerical values were obtained according to eqs. (20-30) of ref. [30] and the data compilation of ref. [39] for $A>4$. For ^{3}He, R has been fixed according to ref. [47].

TAB. VI

Reaction cross sections (mb) on ^{3}He and ^{4}He calculated with the Glauber model in correspondence with two different values of the β^2_j parameters in $(GeV/c)^{-2}$. For a comparison, also the experimental values of the reaction cross section on ^{3}He [44] and on ^{4}He [45] are reported.

FIGURE CAPTIONS

Fig. 1 ρ_p measurements from various experiments. (o): pre-Lear data [10,12-14]; (∇): (ref. [2]; (•): ref. [3]; (▲): ref. [1,4]; (□): ref. [8].

Fig. 2 $\bar{n}p(\bar{p}n)$ total cross section. (o) Experimental points from ref. [36]. ( ) Determination of $\bar{p}n$ total cross section at 600 MeV/c and 300 MeV/c from ref. [30].

Fig. 3 Elastic differential cross section for $\bar{p}$-^{12}C (a) and $\bar{p}$-^{40}Ca (b) at 300 MeV/c. The solid curves refer to $\rho=\varepsilon=0$, the dashed curves to $\rho=\varepsilon=-0.25$, the dotted curves to pure nuclear scattering and the dash-dotted curves to pure Coulomb scattering on a point-like charge Ze (from ref. [15]).

Fig. 4 a) - The same as fig. 3a but for $\bar{p}$-^{12}C elastic scattering at 600 MeV/c and $\rho=\varepsilon=0.2$. b) - The same as in fig. 3a but for $\bar{p}$-^{40}Ca elastic scattering at 600 MeV/c and $\rho=\varepsilon=0.2$ (from ref. [15]).

Fig. 5 Differential elastic cross sections for $\bar{p}$-^{12}C (a) and $\bar{p}$-^{40}Ca (b) at 600 MeV/c. The input parameters come from ref. [15] (see tab. II), the model is that of ref. [30].

Fig. 6 Differential elastic cross sections for $\bar{p}$-^{12}C (a) and $\bar{p}$-^{40}Ca (b) at 300 MeV/c. The input parameters come from ref. [15] (see tab. II), the model is that of ref. [30]. The solid curves refer to $\rho=\rho_p=\rho_n=0$ and the dotted to $\rho=\rho_p=\rho_n=-0.25$.

Fig. 7 Differential elastic cross section for $\bar{p}$-^{40}Ca at 600 MeV/c. The model is that of ref. [30], the input parameters come from ref. [15]. The solid curve is obtained performing the smoothing of the theoretical cross section over the detector resolution (see formula (3.3) and fig. 4b), the dotted one corresponds to the theoretical cross section without the smoothing.

Fig. 8 Differential elastic cross sections for $\bar{p}$-^{40}Ca at 300 MeV/c with the input parameters of ref. [15] and the model of ref. [30]. (a) the ρ parameter is $\rho_p=\rho_n=0.0$; (b): the ρ parameter is $\rho_p=\rho_n=-0.25$. The solid curves [the same as in fig. 6b] correspond to the correct treatment of the smoothing of the theoretical cross sections and of the Coulomb phase; the dotted lines are obtained without the smoothing of the theoretical cross section, the dashed line is obtained by using also the approximate formula of ref. [32] for the Coulomb phase.

Fig. 9 Differential elastic cross sections for $\bar{p}$-^{18}O (a) and $\bar{p}$-^{208}Pb (b) at 600 MeV/c. The $\bar{p}$-nucleon parameters are the best fit parameters of ref. [30] (see tab. II) and the nuclear shape parameters are taken from tab. III.

Fig. 10 Differential elastic cross sections for $\bar{p}$-^{12}C and $\bar{p}$-^{40}Ca at 300 MeV/c obtained by a simultaneous fit on both nuclei. σ_n was fixed at 214 mb and the best fit values of β^2_n and ρ_n are given in tab. IV, row f. The $\bar{p}$-proton parameters are those of tab. II, part (a) and the nuclear shape parameters are those of tab. I, part (a). The figure is taken from ref. [41].

Fig. 11 Reaction cross sections on different nuclei at 200, 300, 600 MeV/c versus $A^{2/3}$. (•) Refs. [18, 43-45]; (o) Ref. [29]; (□) Ref. [46].

TABLE I

			(a) ref. [30]	(b) ref. [15]	
(fm)	^{12}C	^{16}O	^{40}Ca	^{12}C	^{40}Ca
R	1.62	1.76	3.70	1.58	3.66
a	--	--	0.507	--	0.545
R_{ch}	1.75	1.89	R	R	R
a_{ch}	--	--	0.550	--	a

TABLE II

	(a) ref. [30]		(b) ref. [15]	
	302 MeV/c	607 MeV/c	302 MeV/c	607 MeV/c
σ_p	238.0	149.2	240.	157.
ρ_p	-0.132	0.216	0.0(-0.25)†	0.2
β^2_p	35.6	20.5	35.6	22.2
σ_n	*177.7±8.2	*135.2±2.0	200.	136.
ρ_n	---	*0.035±0.017	ρ_p	ρ_p
β^2_n	*32.4±2.5	*21.8±0.6	β^2_p	β^2_p

TABLE III

fm	^{18}O	^{208}Pb
R	2.61	7.17
a	.496	0.485
R_{ch}	2.61	6.64
a_{ch}	.513	0.540

TABLE IV

row	nucleus	Energy (MeV)	ρ_p	β^2_n	ρ_n	χ^2/DF	DF
a	^{12}C	46.8		25.7±1.4	0.003±0.050	1.39	42
b	^{40}Ca	47.8	0.0	25.9±2.1	-0.414±0.063	1.94	22
c	^{12}C, ^{40}Ca	a+b		25.3±1.2	-0.292±0.060	1.89	66
d	^{12}C	46.8		25.6±1.4	0.185±0.050	1.38	42
e	^{40}Ca	47.8	-0.132	25.3±2.5	-0.236±0.060	1.92	22
f	^{12}C, ^{40}Ca	d+e		25.1±1.3	-0.110±0.060	1.88	66

TABLE V

fm	^{3}He	^{4}He	^{12}C	^{16}O	^{20}Ne	^{27}Al	^{40}Ca	^{63}Cu
R	1.56	1.37	1.62	1.76	R_{ch}	R_{ch}	R_{ch}	R_{ch}
a	--	--	--	--	0.52	0.52	0.51	0.56
R_{ch}	1.70	1.53	1.75	1.89	2.74	2.84	3.70	4.21
a_{ch}	--	--	--	--	0.57	0.57	0.55	0.59

TABLE VI

β^2_p	73.		48.
β^2_n	60.		39.
$\sigma_R(^3He)$	466.		393.
$\sigma_R(^4He)$	502.		414.
$\sigma^{exp}_R(^3He)$		392.4±23.8	
$\sigma^{exp}_R(^4He)$		405.6±16.4	

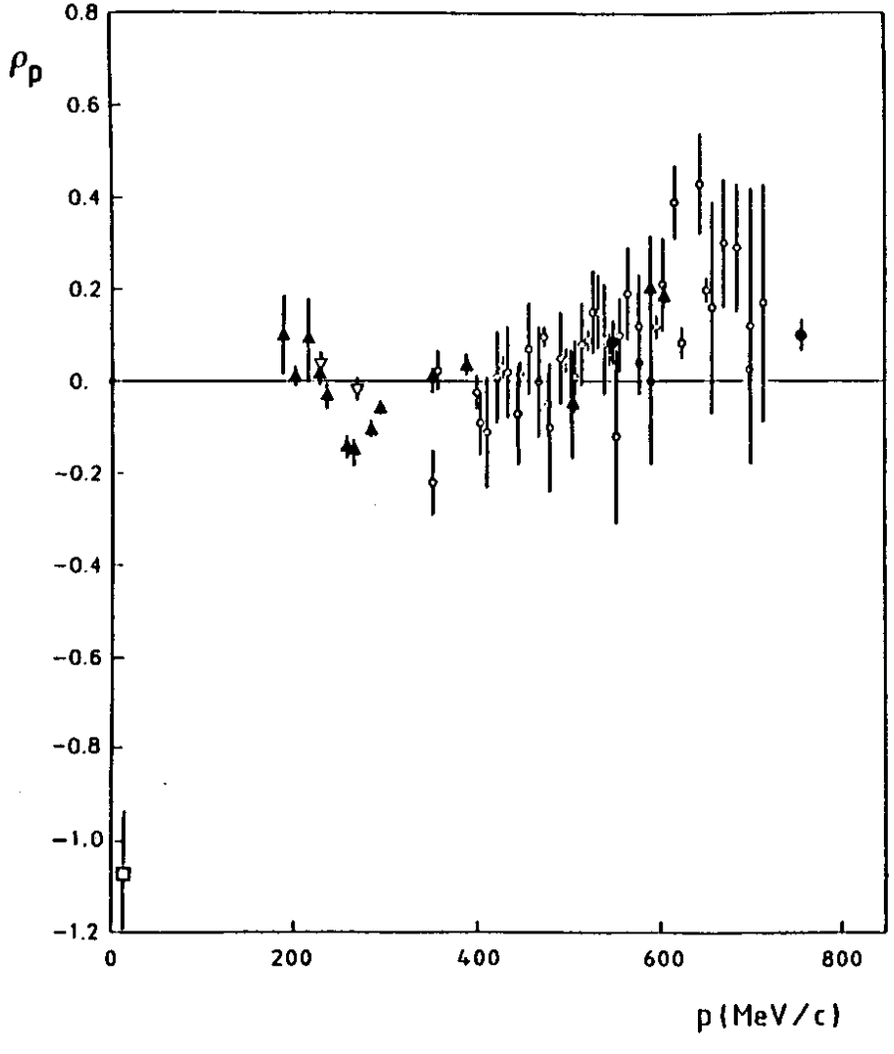
ρ_p
0.8
0.6
0.4
0.2
0.
-0.2
-0.4
-0.6
-0.8
-1.0
-1.2
0
200
400
600
800
p (MeV/c)

Fig. 1

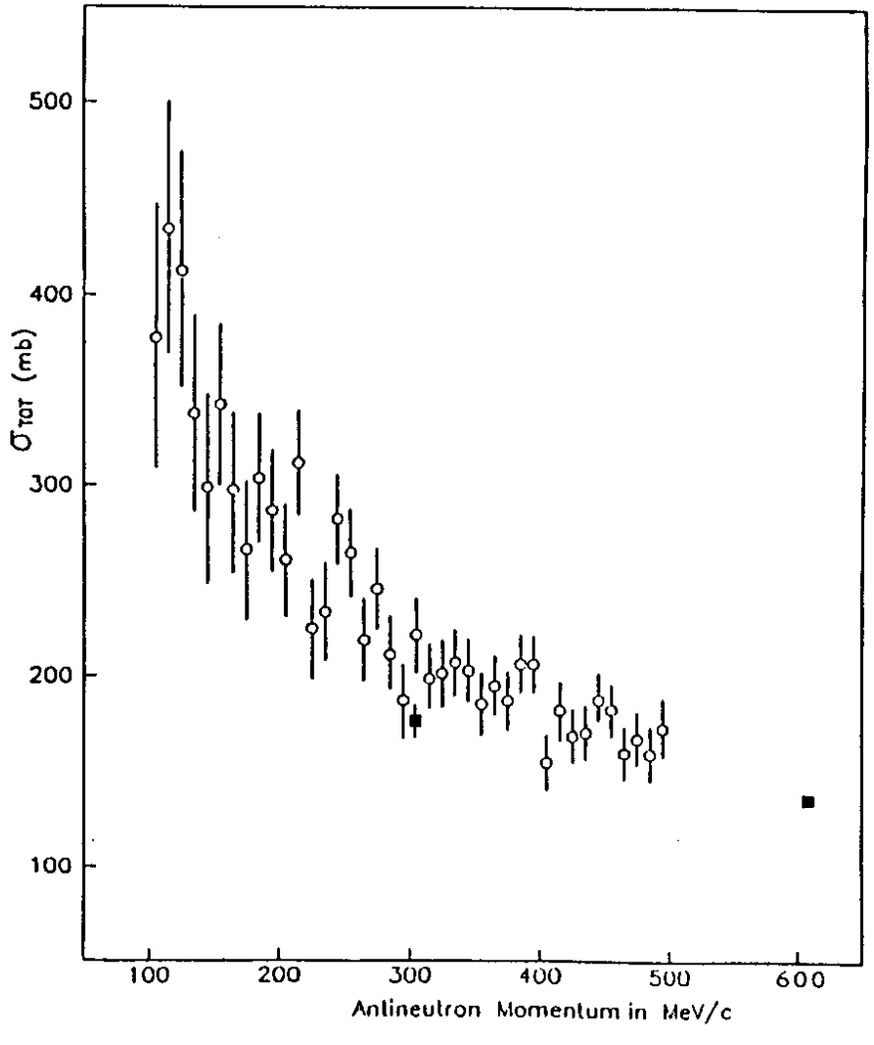
σ_{tot} (mb)
500
400
300
200
100
100
200
300
400
500
600
Antineutron Momentum in MeV/c

Fig. 2

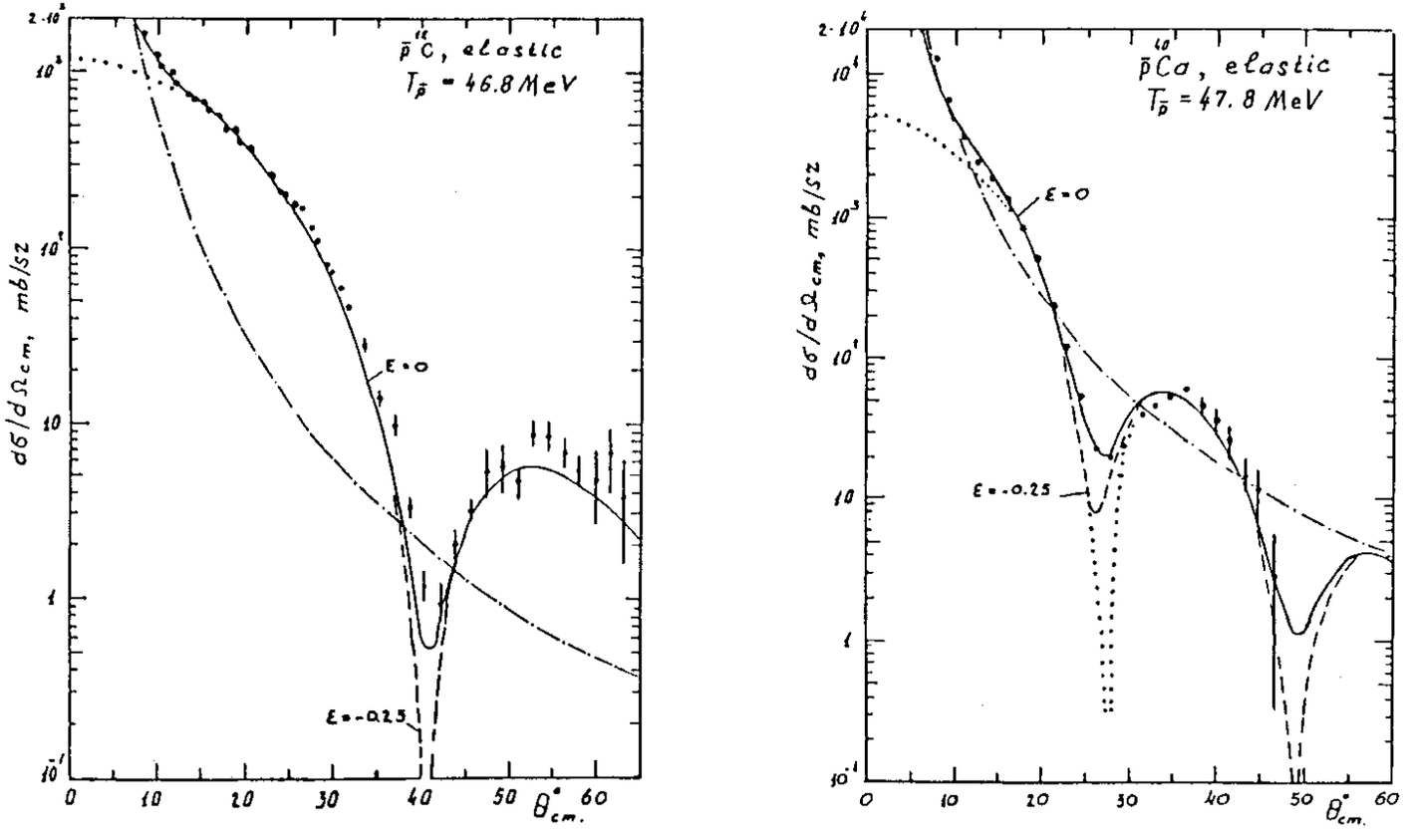
$\bar{p}^{12}C$, elastic
$T_{\bar{p}}$ = 46.8 MeV
ε = 0
ε = -0.25
$d\sigma/d\Omega_{cm}$, mb/sr
$\theta^{\circ}_{cm.}$
$\bar{p}^{40}Ca$, elastic
$T_{\bar{p}}$ = 47.8 MeV
ε = 0
ε = -0.25
$d\sigma/d\Omega_{cm}$, mb/sr
$\theta^{\circ}_{cm.}$

a) b)

Fig. 3

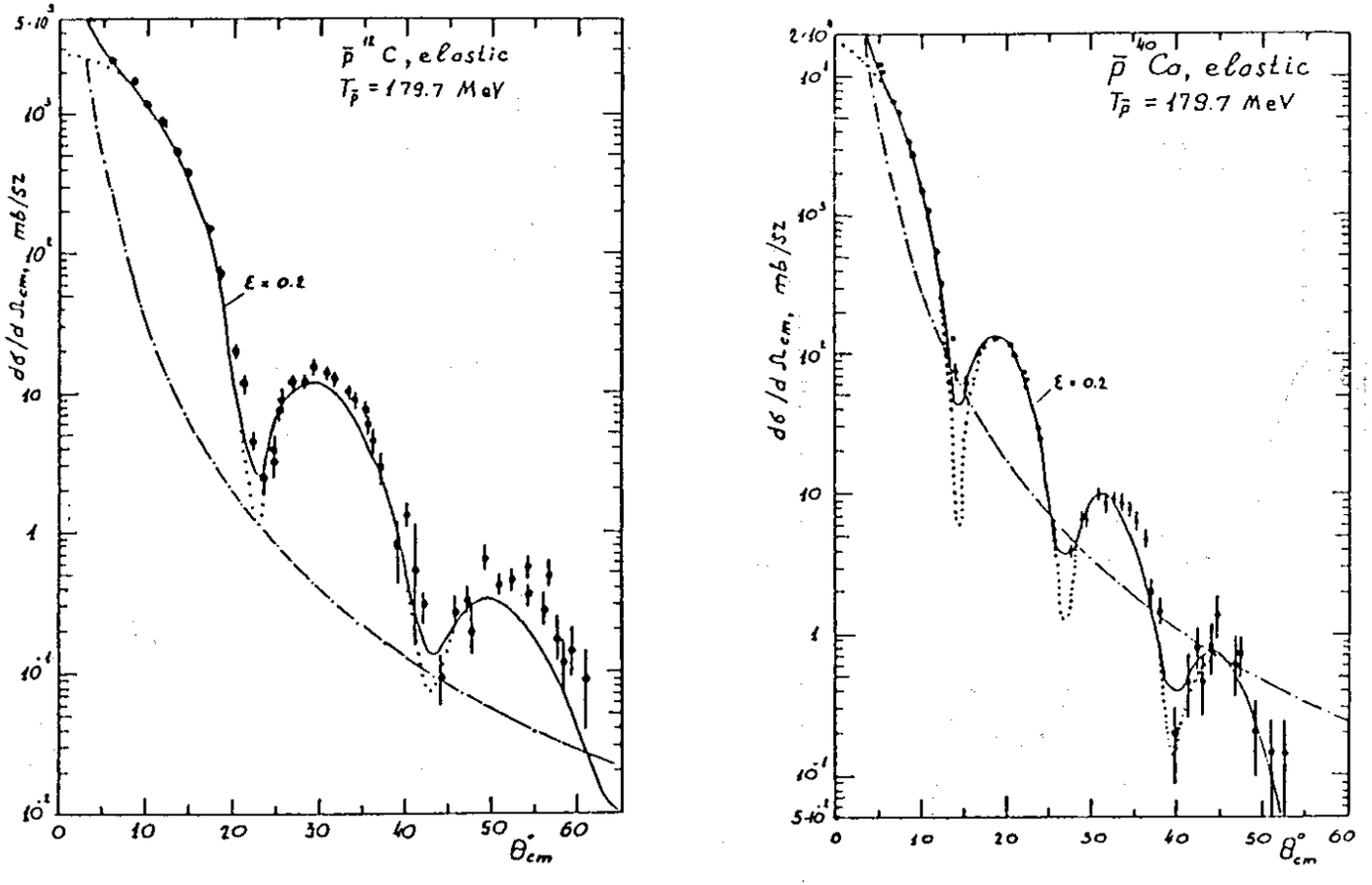
$\bar{p}$ ^{12}C, elastic
$T_{\bar{p}}$ = 179.7 MeV
ε = 0.2
dσ/dΩ$_{cm}$, mb/sr
θ°_{cm}
$\bar{p}$ ^{40}Ca, elastic
$T_{\bar{p}}$ = 179.7 MeV
ε = 0.2
dσ/dΩ$_{cm}$, mb/sr
θ°_{cm}

a) b)

Fig. 4

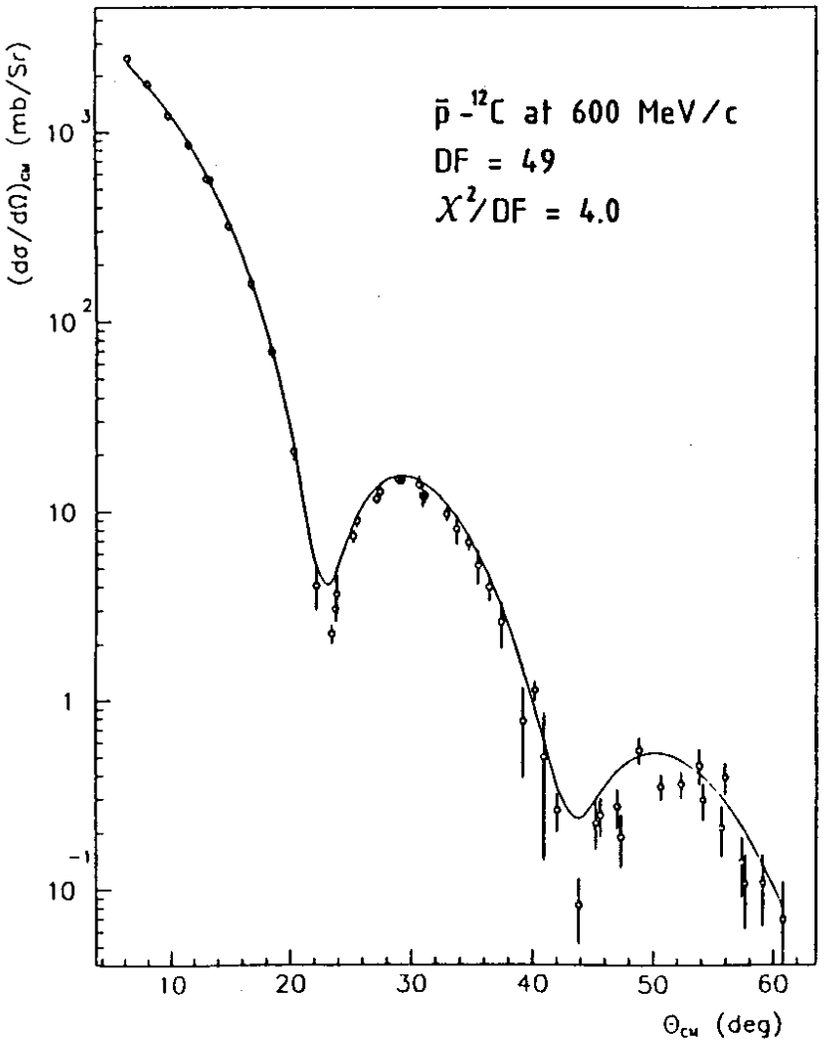
$\bar{p}$ - ^{12}C at 600 MeV/c
DF = 49
χ^2/DF = 4.0
$(d\sigma/d\Omega)_{cm}$ (mb/Sr)
Θ_{cm} (deg)

Fig. 5a

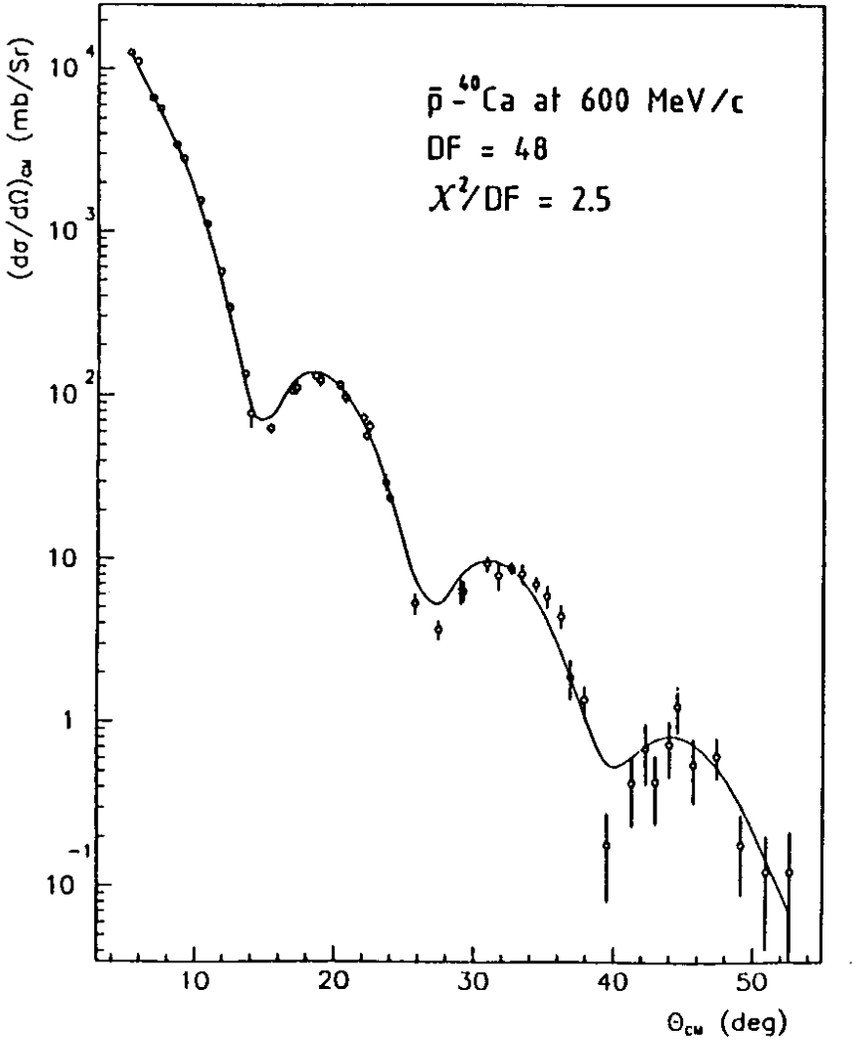
$\bar{p}$ - ^{40}Ca at 600 MeV/c
DF = 48
χ^2/DF = 2.5
$(d\sigma/d\Omega)_{cm}$ (mb/Sr)
Θ_{cm} (deg)

Fig. 5b

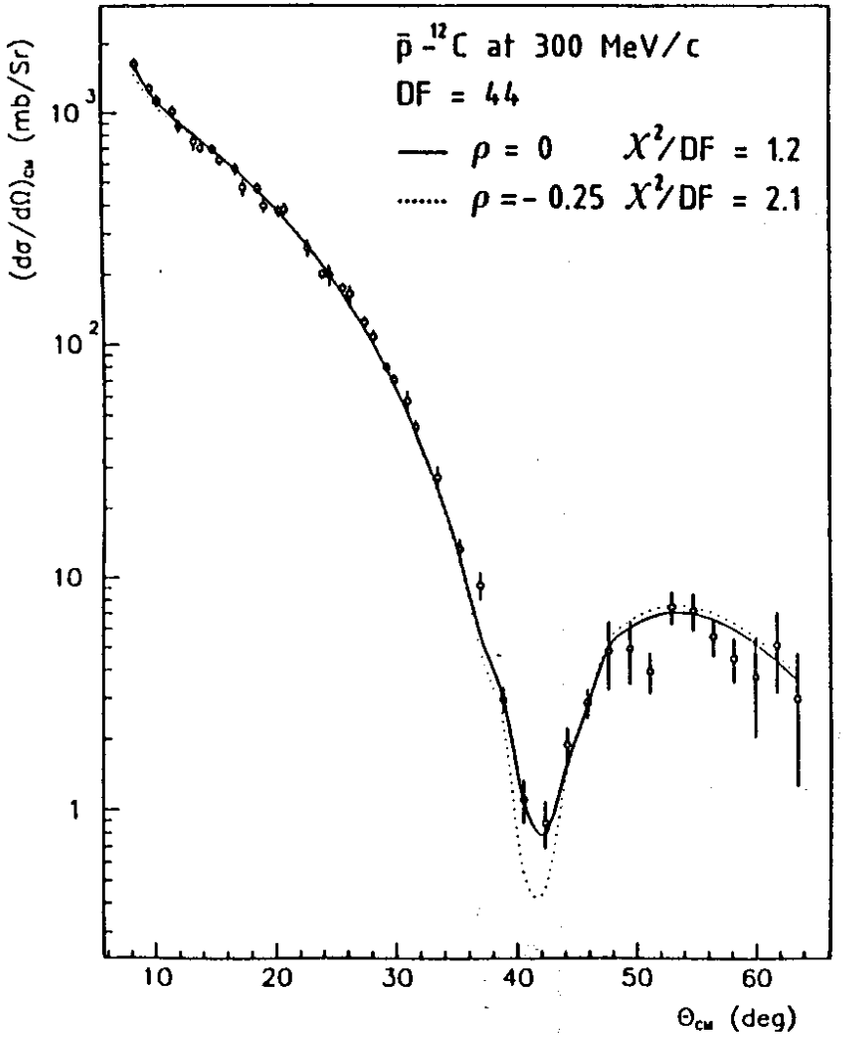
$\bar{p}$ - ^{12}C at 300 MeV/c
DF = 44
—— ρ = 0 χ^2/DF = 1.2
····· ρ = - 0.25 χ^2/DF = 2.1
$(d\sigma/d\Omega)_{cm}$ (mb/Sr)
10^3
10^2
10
1
10
20
30
40
50
60
Θ_{cm} (deg)

Fig. 6a

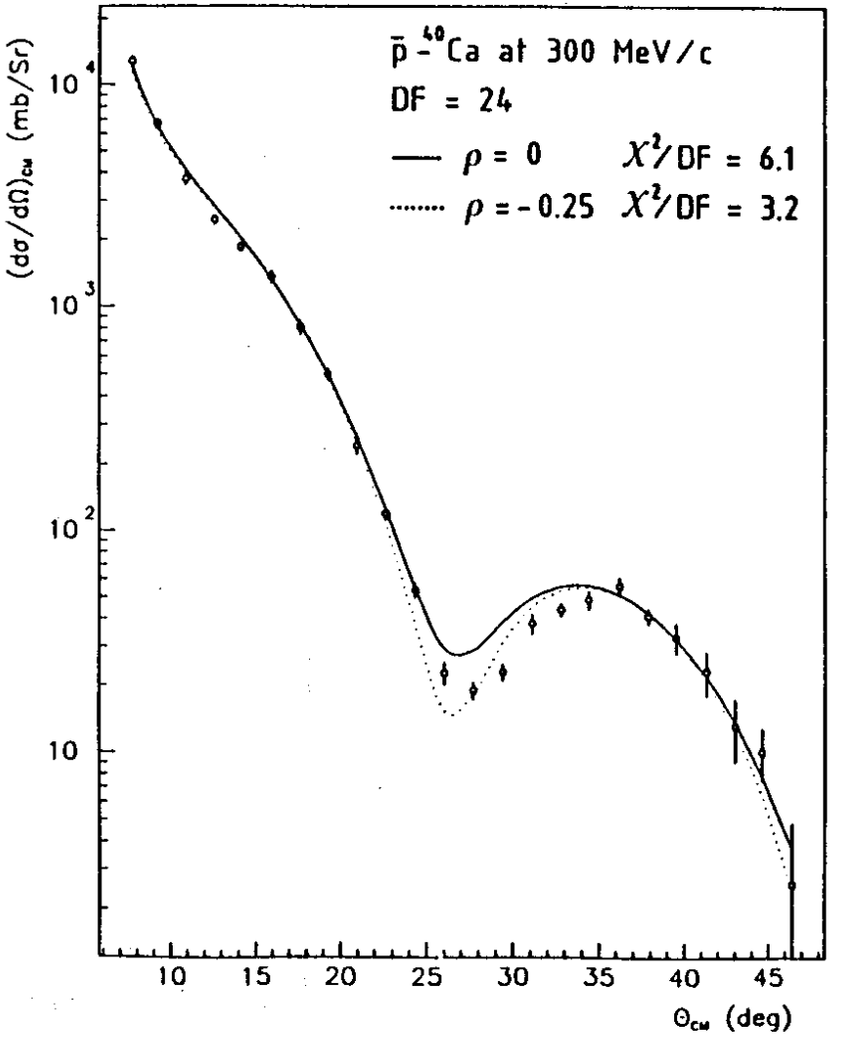
$\bar{p}$ - ^{40}Ca at 300 MeV/c
DF = 24
—— ρ = 0 χ^2/DF = 6.1
····· ρ = - 0.25 χ^2/DF = 3.2
$(d\sigma/d\Omega)_{cm}$ (mb/Sr)
10^4
10^3
10^2
10
10
15
20
25
30
35
40
45
Θ_{cm} (deg)

Fig. 6b

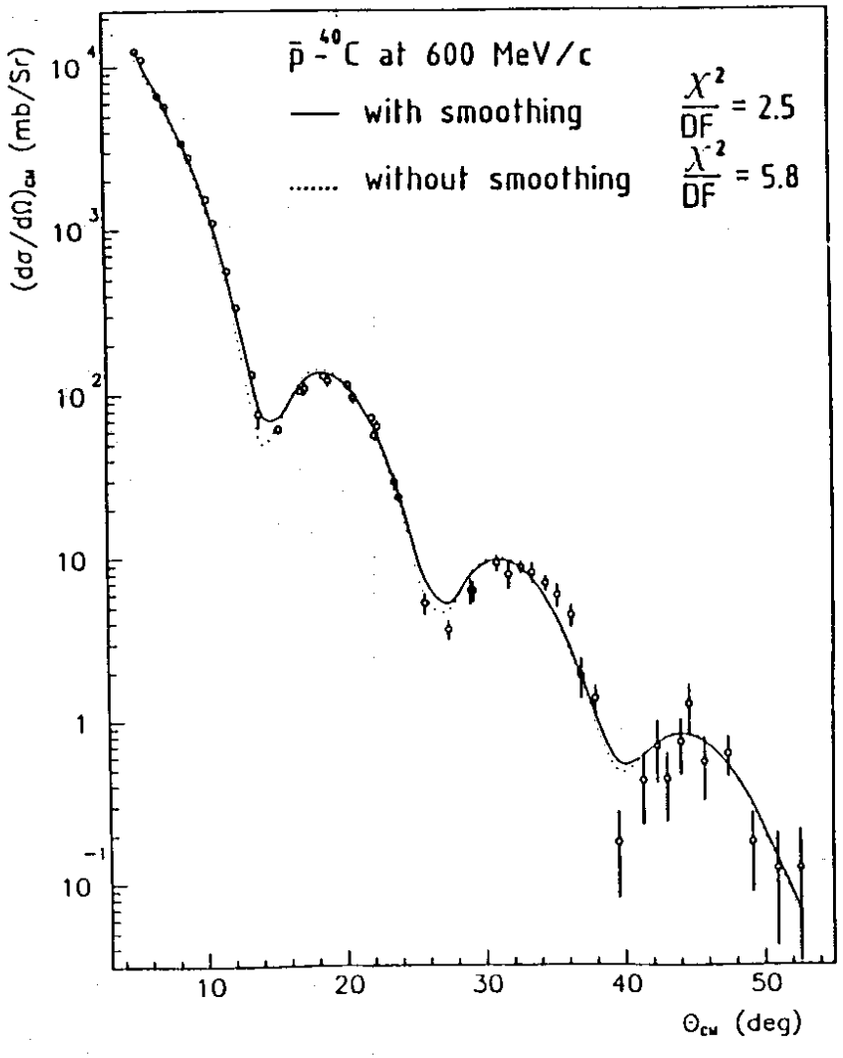
$\bar{p}$ - ^{40}C at 600 MeV/c
with smoothing
without smoothing
$\frac{\chi^2}{DF}$ = 2.5
$\frac{\chi^2}{DF}$ = 5.8
$(d\sigma/d\Omega)_{cm}$ (mb/Sr)
10^4
10^3
10^2
10
1
10^{-1}
10
20
30
40
50
Θ_{cm} (deg)

Fig. 7

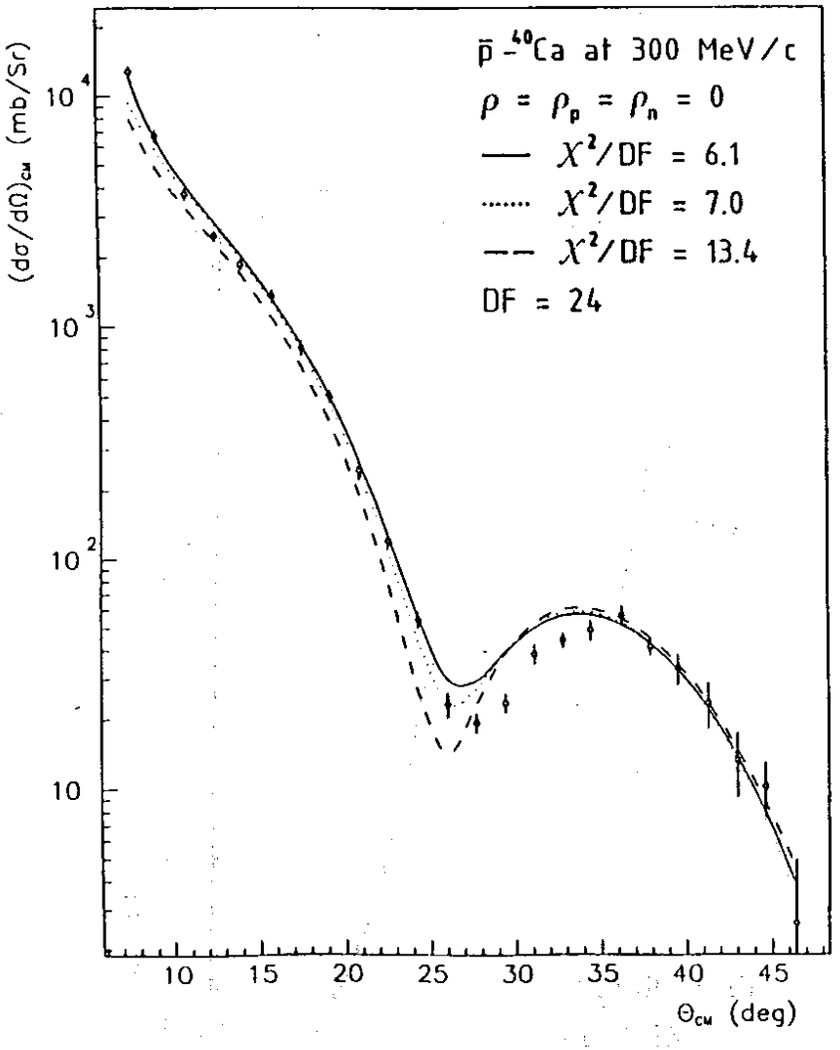
$\bar{p}$ - ^{40}Ca at 300 MeV/c
$\rho = \rho_p = \rho_n = 0$
χ^2/DF = 6.1
χ^2/DF = 7.0
χ^2/DF = 13.4
DF = 24
$(d\sigma/d\Omega)_{cm}$ (mb/Sr)
Θ_{cm} (deg)

Fig. 8a

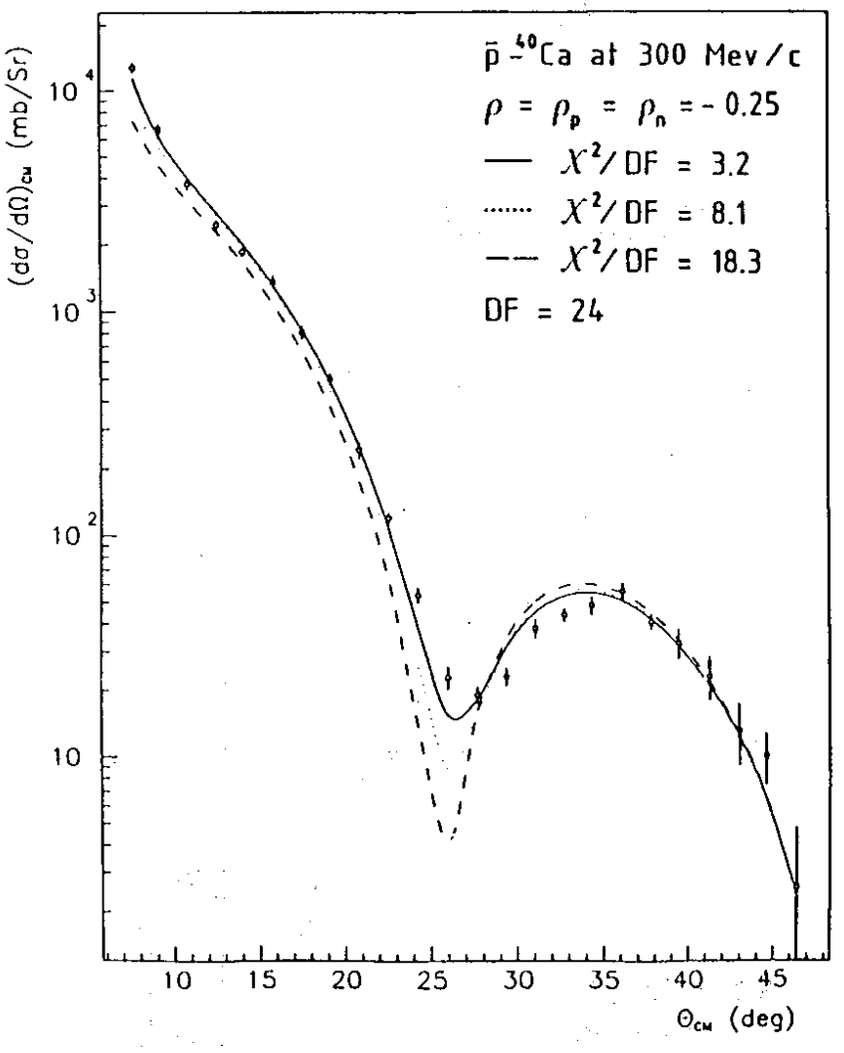
$\bar{p}$ - ^{40}Ca at 300 Mev/c
$\rho = \rho_p = \rho_n = -0.25$
χ^2/DF = 3.2
χ^2/DF = 8.1
χ^2/DF = 18.3
DF = 24
$(d\sigma/d\Omega)_{cm}$ (mb/Sr)
Θ_{cm} (deg)

Fig. 8b

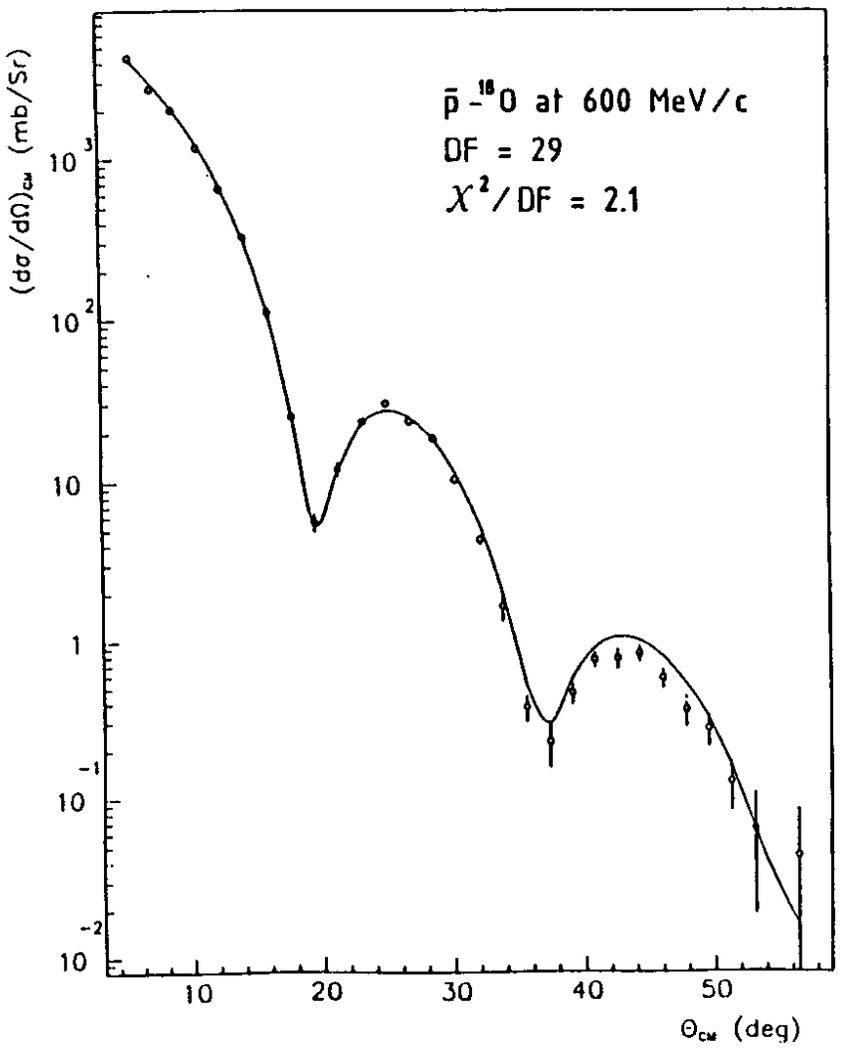
$\bar{p}$ - ^{18}O at 600 MeV/c
DF = 29
χ^2/DF = 2.1
$(d\sigma/d\Omega)_{cm}$ (mb/Sr)
Θ_{cm} (deg)

Fig. 9a

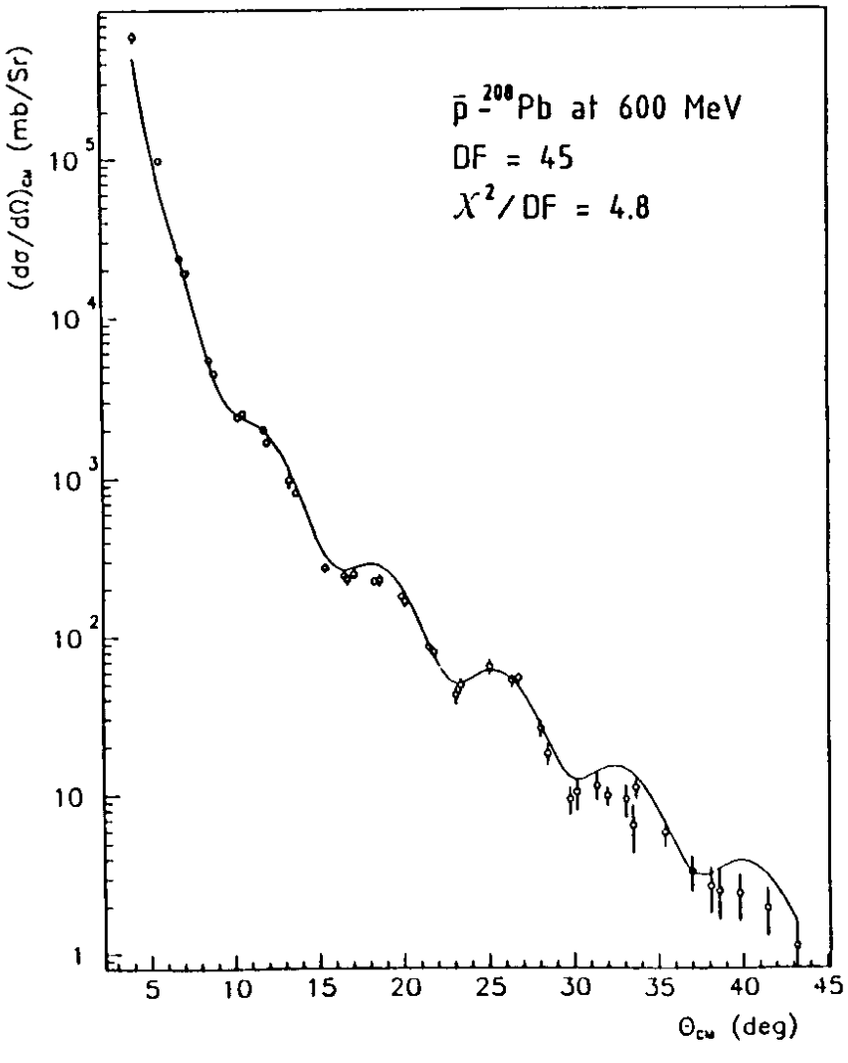
$\bar{p}$ - ^{208}Pb at 600 MeV
DF = 45
χ^2/DF = 4.8
$(d\sigma/d\Omega)_{cm}$ (mb/Sr)
Θ_{cm} (deg)

Fig. 9b

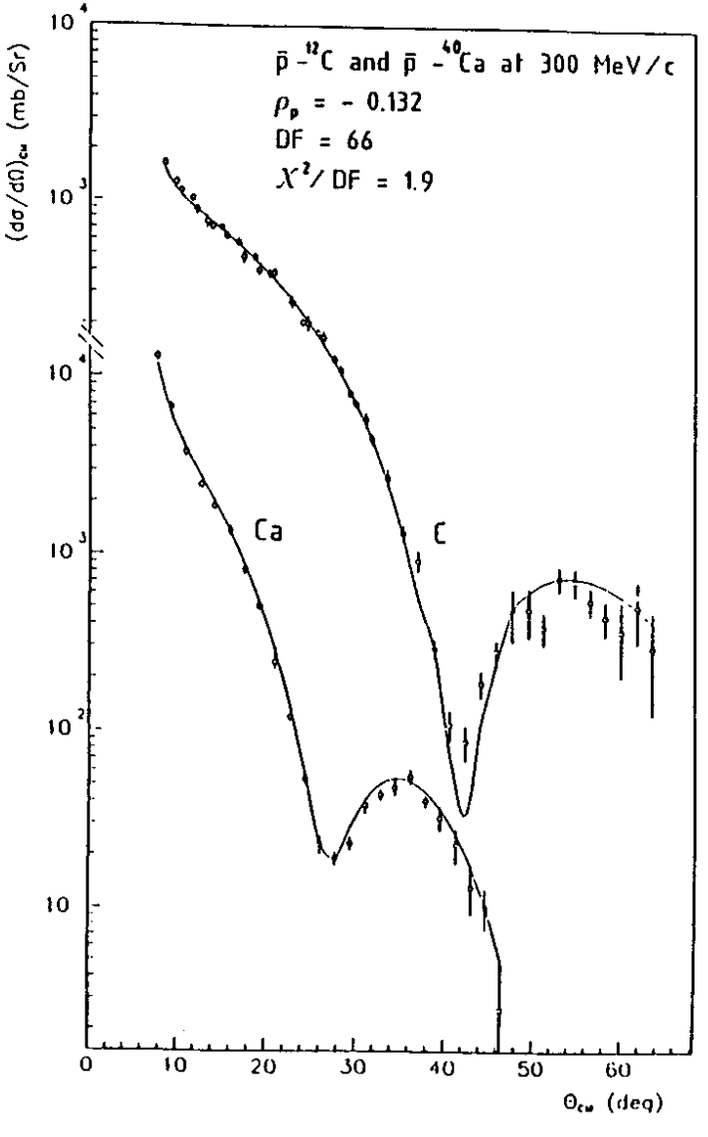
$\bar{p}$ - ^{12}C and $\bar{p}$ - ^{40}Ca at 300 MeV/c
ρ_p = - 0.132
DF = 66
χ^2/DF = 1.9
Ca
C
$(d\sigma/d\Omega)_{cm}$ (mb/Sr)
Θ_{cm} (deg)

Fig. 10

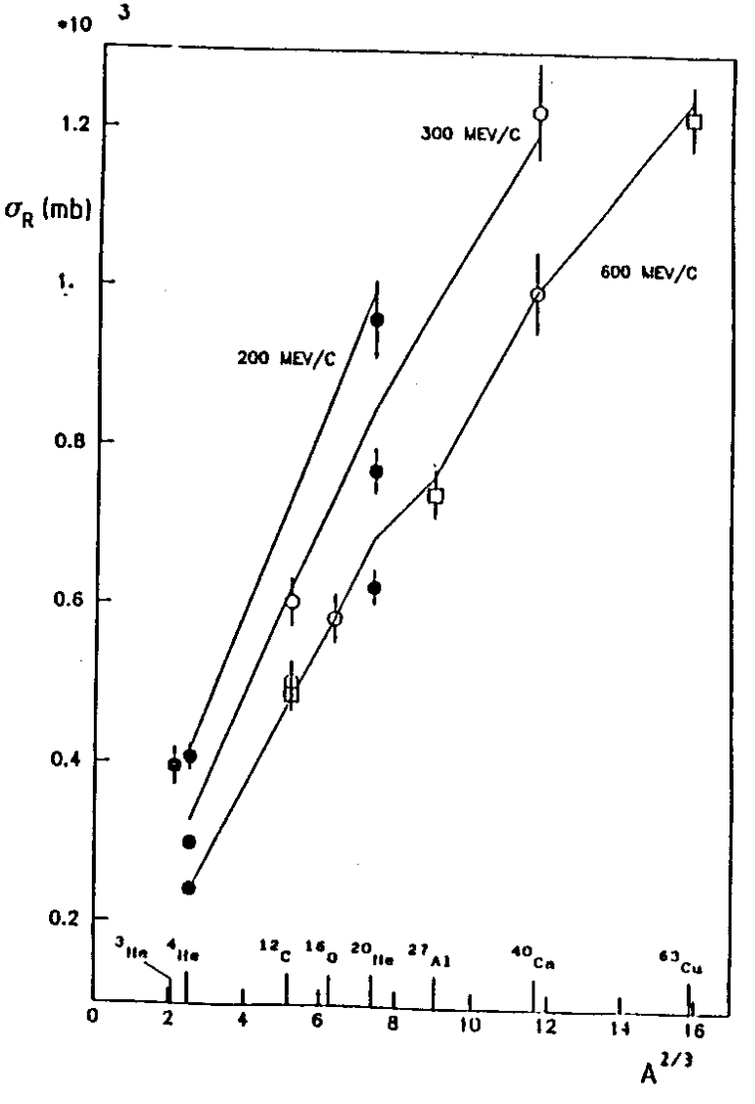
σ_R (mb)
300 MEV/C
600 MEV/C
200 MEV/C
^{3}He ^{4}He ^{12}C ^{16}O ^{20}Ne ^{27}Al ^{40}Ca ^{63}Cu
$A^{2/3}$

Fig. 11